NASA CR-50001
BATT-4673-T2

DEVELOPMENT OF A VAPOR-PRESSURE-OPERATED HIGH-TEMPERATURE SENSOR DEVICE

by

J. R. Van Orsdel, G. E. Raines, and J. M. Allen

prepared for

NATIONAL AERONAUTICS AND SPACE ADMINISTRATION

CONTRACT NAS 3-5202

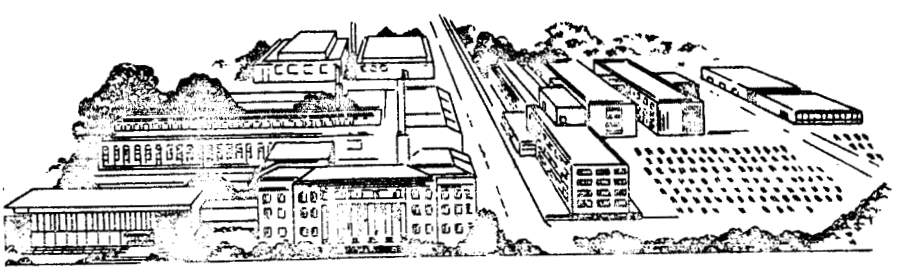

BATTELLE
MEMORIAL INSTITUTE

NOTICE

This report was prepared as an account of Government sponsored work. Neither the United States, nor the National Aeronautics and Space Administration (NASA), nor any person acting on behalf of NASA:

A.) Makes any warranty or representation, expressed or implied, with respect to the accuracy, completeness, or usefulness of the information contained in this report, or that the use of any information, apparatus, method, or process disclosed in this report may not infringe privately owned rights; or

B.) Assumes any liabilities with respect to the use of, or for damages resulting from the use of any information, apparatus, method or process disclosed in this report.

As used above, "person acting on behalf of NASA" includes any employee or contractor of NASA, or employee of such contractor, to the extent that such employee or contractor of NASA, or employee of such contractor prepares, disseminates, or provides access to, any information pursuant to his employment or contract with NASA, or his employment with such contractor.

Requests for copies of this report should be referred to:

National Aeronautics and Space Administration
Office of Scientific and Technical Information
Washington 25, D.C.
Attention: AFSS-A

15517

SECOND QUARTERLY REPORT
(June 12 through September 11, 1964)

DEVELOPMENT OF A VAPOR-PRESSURE-OPERATED HIGH-TEMPERATURE SENSOR DEVICE

by

J. R. Van Orsdel, G. E. Raines,
and J. M. Allen

prepared for

National Aeronautics and Space Administration

September 11, 1964

Contract NAS3-5202

Technical Management
NASA – Lewis Research Center
Cleveland, Ohio
Advanced Development and Evaluation Division
Miles O. Dustin

BATTELLE MEMORIAL INSTITUTE
505 King Avenue
Columbus, Ohio 43201

TABLE OF CONTENTS

LIST OF TABLES

LIST OF FIGURES

LIST OF FIGURES
(Continued)

DEVELOPMENT OF A VAPOR-PRESSURE-OPERATED HIGH-TEMPERATURE SENSOR DEVICE

by

J. R. Van Orsdel, G. E. Raines,
and J. M. Allen

SUMMARY

32631

Initial studies of compatibility between candidate probe materials and liquid-metal charging fluids have been completed. Tungsten-3% rhenium-lead, tungsten-bismuth, and tungsten-25% rhenium-lead appear most attractive in decreasing order.

The probe size of 1/8-inch ID x 1/4-inch OD x 1-1/2 inches long has been found satisfactory on geometrical considerations and by thermal analysis.

A preliminary design study of the signal generating system directs future development to the null-point pneumatically balanced diaphragm.

The effects of internal heat generation and radiative heat loss on response have been further elucidated. The time constant has been found to become increasingly higher at the highest temperatures. This characteristic would be encountered in any similar type of probe sensor such as a thermocouple.

Work in the third quarter will consist of extensive studies of hydrogen diffusion through the probe walls at high temperature and extended-time compatibility tests between the container and charging alloy. A signal detector for attachment to the probe will be built and characterized at the bench.

INTRODUCTION

The development of a vapor-pressure-operated temperature sensor (depicted schematically in the first quarterly report) for use at temperatures up to 5000 R is hindered considerably by the scarcity of materials with sufficient strength and by the lack of compatibility of these materials toward a suitable liquid-metal pressure-generating medium. Candidate structural materials for the probe were selected on the basis of existing, though limited, elevated-temperature data. The liquid metals chosen for study were selected chiefly on the basis of their vapor pressures over the temperature range of 3000 to 5000 R. Therefore, the most pressing need in the initial development of the sensor is the discovery of a compatible metal – liquid-metal system. Very little is known in this area at the high temperatures of interest; therefore compatibility tests have been in progress to discover the most promising metals system.

In addition to compatibility testing, studies in engineering design are in progress as an aid to constructing the pressure readout system for attachment to the sensor probe.

Heat-transfer analyses are being continued to establish the probable response time and sensitivity of the device in its intended environment.

PROBE MATERIALS

A search of the literature during the past quarter suggested the following list of metals as probe material candidates:

Molybdenum – 30% tungsten
Tungsten
Tungsten – 3% Rhenium
Tungsten – 25% Rhenium
Rhenium
Tantalum – 5% tungsten – 2.5% molybdenum
Tantalum – 8% tungsten – 2% hafnium
Tantalum – 10% tungsten – 2.5% hafnium
Tantalum – 10% tungsten – 2.5% molybdenum

These nine metals and alloys were believed to have the most to offer as probe materials. Of these, the tantalum alloys are of questionable value because of tantalum's ability to dissolve hydrogen at intermediate temperatures. Also, elevated-temperature data in DMIC Report 189(1) suggest that they probably are not strong enough to resist creep and rupture at 5000 R. Therefore, they are being dropped from further consideration in favor of tungsten and rhenium metals and their alloys.

COMPATIBILITY STUDIES

Compatibility testing in the range 4500 to 5000 R was continued this quarter; induction heating and a hydrogen atmosphere at atmospheric pressure were used. The equipment, testing procedure, and specimen configuration were reported in the First Quarterly Report.

It was necessary to make two refinements in the second quarter. The induction heating coil now consists of 11 flattened turns of 1/4-inch-diameter copper tubing and is 2-3/8 inches long. The inside diameter of the coil is 3/4 inch. The increased number of turns, over the original 5 turns, made heating to 5000 R possible with about 3600 volts at 500 kc. Formerly, voltages often ran as high as 9000 v and were prone to arc to the specimen.

The specimen style has been changed slightly in the interest of material economy. Figure 1 is a portrayal of these new specimens and the method of holding during heating. The specimen is 1-1/2 inches long with a 1/8-inch hole drilled 1-1/8 inches deep from one end. After the charging metal is placed in the hollow specimen, the end is closed by electron-beam welding. The latter is the same procedure used on the longer specimens in the first quarter.

(1) Schmidt, F. F., and Ogden, H. R., "The Engineering Properties of Tantalum and Tantalum Alloys", DMIC Report 189, Battelle Memorial Institute (September 13, 1963).

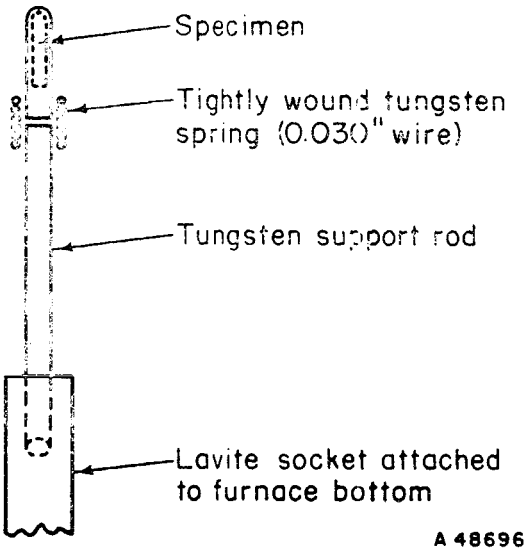

FIGURE 1. REVISED SPECIMEN AND METHOD OF HOLDING FOR HIGH-TEMPERATURE TESTING

Table 1 lists the results from compatibility tests on probe materials to date. The table includes those tests run during the first quarter that displayed some possibilities.

Photomicrographs of sectioned Specimens 14 through 28 are in the Appendix, Figures A-1 through A-14.

Interpretation of Metallographic Observations

The photomicrographs showing the effects of high temperature on the candidate probe materials in contact with bismuth, lead, and antimony reveal that susceptibility to attack by the liquid metals is most prevalent in the grain boundaries. This condition is believed to stem from the probable existence of impurities such as oxygen at these locations. Therefore, the pure metals tungsten and rhenium are of doubtful reliability for use as probe materials because they tend to reject oxides to their grain boundaries.

The W-3Re alloy failed by grain-boundary attack, much more quickly than pure tungsten, when exposed to bismuth and antimony. The intergranular nature of the failure suggests a stress-corrosion phenomenon which often occurs in alloys by solution of a minor phase present in the grain boundary. Thus, a little bit of alloying of tungsten with rhenium was detrimental except in the case of lead. In this case, lead did not find a soluble material at the grain boundaries, and the W-3Re alloy was able to complete 1 hour at 5000 R without failure.

Tests on unalloyed rhenium were conducted in contact with bismuth and lead at 5000 R. In both cases, considerable grain-boundary penetration developed, although no swelling or bursting of the specimens occurred.

TABLE 1. SUMMARY OF COMPATIBILITY TESTS

Specimen	Material	Exposure Temp, R	Exposure Time, minutes	Results
		Tests During First Quarter		
4	Mo-30W; Pb	4000	60	No reaction, no leaking
7	Mo-30W; Pb	4500	60	Some reaction, no leaking
8	W; Bi	4500	60	No reaction, no leaking
9	W; Bi	5000	10	No reaction, leak at weld
10	W; Pb	4500	60	Moderate reaction, no leaking
11	W; Pb	4700	25	Severe reaction, leaking
12	W; Sb	4500	60	Minor reaction, no leaking
13	W; Sb	5000	15	Minor reaction, leaking
		Tests During This Quarter		
14	Mo-30W; Sb	4500	5	Specimen ruptured
15	W-3Re; Bi	4500	3	Specimen ruptured
16	Repeat	No. 15		Same results
17	W-3Re; Sb	4500	60	No leaking
18	W-3Re; Sb	5000	5	Specimen ruptured
19	W-3Re; Pb	4500	60	No leaking
20	W-3Re; Pb	5000	60	Ditto
21	W-25Re; Pb	4500	60	"
22	W-25Re; Pb	5000	60	"
23	W-25Re; Sb	4500	60	"
24	W-25Re; Sb	5000	60	Sample bulged 0.006 inch on diam, or 2.4 per cent
25	W-25Re; Bi	4500	60	No leaking
26	W-25Re; Bi	5000	50	Sample buldged about 50 per cent in diam, then ruptured
27	Re; Pb	5000	60	No leaking
28	Re; Bi	5000	60	No leaking

The W-25Re alloy exhibited the greatest resistance to attack by the liquid metals but, unfortunately, displayed a lack of sufficient creep resistance. Specimens 24 and 26 both increased in diameter during testing at 5000 R (Table 1). The final diameters of Specimens 21 and 22 containing lead did not indicate creep.

Of the specimens evaluated in the 1-hour test at 4500 and 5000 R, three stand out as worthy of further evaluation for this program:

Unalloyed tungsten – bismuth
Tungsten – 3% rhenium – lead
Tungsten – 25% rhenium – lead

These material combinations will be evaluated further during the next quarter.

GAS-PRESSURE-IMPOSED STRESSES

The static stresses imposed on the specimens during compatibility testing are a result of the internal liquid-metal vapor pressure and the external furnace-atmosphere pressure (1 atm). However, the expected application of the sensor specifies an external pressure of 600 psia. Therefore, it is interesting to calculate static stresses arising in the probe owing to these two conditions. Additional stresses arising from high gas velocities and mechanical vibrations will be treated later in the program.

The static stresses are calculated by treating the specimen as a thick-walled cylinder and applying Lamé's solution[1]:

$$\text{Max } S_t = \frac{P_1(r_1^2 + r_2^2) - 2P_2 r_2^2}{r_2^2 - r_1^2} ,$$

where

$\text{Max } S_t$ = maximum circumferential stress

P_1 = internal pressure

P_2 = external pressure

r_1 = radius of specimen bore, 1/16 inch

r_2 = maximum specimen radius, 1/8 inch.

$\text{Max } S_t$ will be positive (tension) or negative (compression), depending upon the relative values of P_1 and P_2. The other stresses arising from the gas pressures are S_r, which is a radial stress, and S_s, which is a shear stress. S_r and S_s were both found by calculation to be of secondary importance relative to max S_t; therefore, they will be ignored for the present.

Calculated values of $\text{Max } S_t$ experienced by the specimens (1/4-inch OD x 1/8-inch ID) during compatibility testing and those that could be expected to arise from an external pressure of 600 psia are given in Table 2.

(1) Resistance of Materials, Seely, Third Edition, p 388.

TABLE 2. STATIC STRESSES (MAX S_t) OWING TO INTERNAL AND EXTERNAL GAS PRESSURES

Charging Metal	Exposure Temp, R	Vapor Pressure (P_1), psia	Max S_t[a], psi	
			P_2 = 14.7 psia	P_2 = 600 psia
Bi	4000	97	122	-1430
	4500	277	422	-1030
	5000	531	848	-704
Sb	4000	51	46	-1500
	4500	142	198	-1355
	5000	277	422	-1030
Pb	4000	40	27	-1520
	4500	117	240	-1395
	5000	240	361	-1190

(a) Positive values of stress are tension, negative values are compression.

Examination of Table 2 reveals that the static stresses in the probe will be largest and compressive when the external atmosphere is 600 psia. This is thought to be a favorable circumstance providing the compressive stress is not sufficient to collapse the probe.

A review of elevated-temperature data reported in the literature on the mechanical properties of the refractory metals is helpful in arriving at the best selection of a probe material. Some recent data on refractory metals are shown in Table 3 for comparative purposes.

TABLE 3. HIGH-TEMPERATURE PROPERTIES OF SOME REFRACTORY METALS

Material	Temp, R	Stress, psi	Time to Effect 2% Strain, hr	Time to Rupture, hr	Elongation in 1-Inch Gage Length, %
W[a]	5172	1000		25.1	5
Re[b]	5172	1000	~3	~20	~14
W-25Re[b]	5172	1000	1	3	10
W-3Re	5172	1000	--	--	--
Ta-10W[b]	5172	1000	0.1	1-1/2	120

(a) High Temperature Materials Program, Progress Report No. 35, Part A, USAEC Contract AT(40-1)-2847, Page 16, Table 2.2.
(b) "Stress-Rupture and Creep Properties of Refractory Metals to 2800 C", General Electric Company USAEC Contract AT(11-1)-171.

Judging from the values given in Table 3, stresses in the probe should be kept below 1000 psi for extended use at 5000 R. It is natural to assume that a more favorable stress level could be achieved by thickening of the probe walls. However, a few sample calculations of stress for different wall thicknesses and bore diameters quickly reveals that a geometry in which the wall thickness equals the radius of the bore is just about

the optimum condition that can be obtained. The following examples are presented for clarification, using 117 psia for P_1, the internal pressure.

Bore Diameter, inches	Probe Diameter, inches	External Pressure, P_2, psia	Max S_t, psi
1/8	1/4	14.7	240
1/8	1/4	600	-1395
1/16	1/4	14.7	101
1/16	1/4	600	-1145
1/8	3/8	14.7	113
1/8	3/8	600	-1200

It is readily seen from the above examples that reducing the bore diameter or increasing the external diameter of the probe has only a negligible effect on lowering the compressive stresses resulting from the high external pressure of 600 psia. Only equalization of internal and external pressures can eliminate stresses of this type in the probe. For this purpose, bismuth (Table 2) would be the best choice of a charging fluid, if compatibility with the container is satisfactory.

Creep is not expected to differ greatly in compression from that in tension because of rapid annealing at the high temperatures involved.

SIGNAL-GENERATING SYSTEM

The temperature sensor under development in this program consists of a hollow probe charged with a liquid metal of favorable vapor pressure over the temperature range of interest and a nonelectrical signal-detection device attached to the cooler end of the probe. This device could be a bellows, Bourdon tube, or elastic diaphragm. After careful consideration of each of the three possibilities, it was decided to concentrate on the elastic diaphragm in the belief that it could be more readily designed to function reliably in the high noise and vibration environment than could the other two.

This section presents the approach used for the diaphragm design, followed by some recommended designs. The recommended designs are considered preliminary, subject to verification of certain material properties and acceptance of the diaphragm deflection sensitivity. Two different types of diaphragms are referred to herein: the null-type diaphragm, which maintains a pressure balance on each side of the diaphragm by means of controlled gas flow, and the mechanical-type diaphragm, which is subjected to pressure on one face only.

Design Considerations

The design pressure for the diaphragm is taken as 20 atmospheres or 294 psi. In the case of the null-type diaphragm, it is assumed that a surge of this magnitude can occur. The design temperature is assumed to be 100 F above the melting point of lead, or 720 F.

Allowable stresses used for the diaphragm are the lower of two values, one-fourth the ultimate tensile strength or one-half the yield strength. The vibration requirements are 4 g's from 10 to 500 cycles per second. Accordingly, the diaphragm is designed with the lowest natural frequency well above 500 cycles per second to avoid a resonance condition. The effect of the liquid metal (mass and damping characteristics) on the diaphragm vibration is neglected.

Material Properties

Ten different materials were selected for the feasibility study, the selection being made primarily on the basis of materials which are compatible with liquid lead according to Reference (1). In some cases, materials were evaluated which were not rated for their compatibility with liquid lead in Reference (1), but in these cases, it was assumed that the material was either compatible with liquid lead, or could be suitably protected.

Table 4 shows the material properties at 720 F which are pertinent to the diaphragm design. The properties of the material used for the final design should be verified for the actual sheet stock used for the diaphragm, since significant variations exist in the properties listed from various sources, especially for the refractory alloys. Only materials with an elongation (at 720 F) of 10 per cent or more were selected for study, to be consistent with the project requirement for high reliability. The data in Table 4 are from References (2), (3), (4), (5), and (6).

Diaphragm Stresses and Deflections

The diaphragm is assumed to be clamped to the diaphragm housing. The equations[7] for the required thickness, t, and the center deflection, δ, are:

$$t = \sqrt{\frac{0.75\, p\, r^2}{S_{max}}} \qquad (1)$$

and

$$\delta = \frac{p\, r^4}{64\, D} \quad , \qquad (2)$$

(1) Liquid Metals Handbook, Second Edition(Revised) June, 1952, Atomic Energy Commission – Department of the Navy.
(2) Metals Handbook, Vol 1, "Properties and Selection of Materials", American Society for Metals, Metals Park, Novelty, Ohio (1961).
(3) Properties of Some Metals and Alloys, The International Nickel Company, Inc., New York, New York.
(4) Schmidt, F. F., and Ogden, H. R., "The Engineering Properties of Tantalum and Tantalum Alloys", DMIC Report 189 (September, 1963).
(5) Schmidt, F. F., and Ogden, H. R., "The Engineering Properties of Tungsten and Tungsten Alloys", DMIC Report 191 (September, 1963).
(6) Beryllium in Aero/Space Structures, The Brush Beryllium Company, Cleveland, Ohio.
(7) Timoshenko, S., and Woinowsky-Krieger, S., Theory of Plates and Shells, McGraw-Hill Book Company, Inc., New York (1959).

TABLE 4. PROPERTIES OF MATERIALS AT 720 F

Material	Density, lb/cu in.	Modulus of Elasticity, 10^6 psi	Melting Point, °F	Ultimate Tensile Strength, 10^3 psi	0.2% Yield Strength, 10^3 psi	Elongation, %
Low-carbon steel	0.29	26	2700	60	25	35
2Cr-1/2Mo steel	0.29	26	2700	64	27	30
4340 steel, 200,000 H. T.	0.29	25	2700	160	120	15
347 stainless steel	0.29	25	2700	67	32	35
Beryllium	0.07	35	2300	45	40	20
Molybdenum	0.37	43	4700	40	20	30
Tantalum	0.60	26	5400	50	35	25
6Al-4V titanium	0.16	13	3000	95	75	15
Tungsten	0.70	46	6100	110	85	10
Zirconium	0.25	10	3400	16	8	50

where

p = 294 psi = uniform pressure

r = radius of circular plate (diaphragm)

σ_{max} = maximum or allowable bending stress

D = flexural rigidity of plate = $\frac{E\,t^3}{12\,(1-\nu^2)}$

t = thickness of plate

E = modulus of elasticity

ν = Poisson's ratio (assume ν = 0.30 for all calculations).

The required diaphragm thickness, calculated from Equation (1), is shown in Table 5 for 1.0- and 2.0-inch-diameter diaphragms. The allowable stress in Equation (1) is assumed to equal the smaller of one-fourth the ultimate tensile strength or one-half the yield strength. Using the required thickness from Equation (1), the maximum deflection at the center of the diaphragm, calculated from Equation (2), is also shown in Table 5.

Natural Frequency of Diaphragm

Timoshenko[1] gives the following equation for the frequency of vibration (w_n, in cycles per second) of a circular plate clamped at its boundary:

$$w_n = \frac{\alpha}{2\pi r^2}\sqrt{\frac{g\,D}{\gamma\,t}} \quad , \tag{3}$$

where

α = constant, based upon the mode of vibration

g = acceleration due to gravity = 386 in./sec^2

γ = density of material.

For the lowest natural frequency of a clamped plate, the constant α = 10.21. The results of Equation (3) are shown in Table 5. The thickness used in Equation (3) is that previously determined from Equation (1).

Diaphragm Considerations

The selection of a preliminary diaphragm design based on the data in Tables 4 and 5 may be dependent on the type of diaphragm to be used. Accordingly, the selection is described for each type diaphragm. In view of the project requirement for high reliability, corrugated diaphragms are not considered acceptable.

(1) Timoshenko, S., Vibration Problems in Engineering, D. Van Nostrand Company, Inc., New York (1955).

TABLE 5. DIAPHRAGM DESIGN[a]

Material	Allowable Stress, ksi	Required Thickness, in.		Maximum Deflection, in.		Natural Frequency, cycles/sec	
		1.00-In. Diameter	2.00-In. Diameter	1.00-In. Diameter	2.00-In. Diameter	1.00-In. Diameter	2.00-In. Diameter
Low-carbon steel	12.5	0.067	0.133	.00040	.00080	24,600	12,300
2Cr-1/2Mo steel	13.5	0.064	0.128	.00046	.00092	23,400	11,700
4340 steel, 200,000 H. T.	40.0	0.037	0.074	.00248	.00496	13,400	6,700
347 stainless steel	16.0	0.058	0.116	.00065	.00130	20,800	10,400
Beryllium	11.5	0.069	0.138	.00027	.00055	59,500	29,800
Molybdenum	10.0	0.074	0.148	.00018	.00036	31,000	15,500
Tantalum	12.5	0.067	0.133	.00040	.00081	17,100	8,600
6Al-4V titanium	24.0	0.048	0.096	.00219	.00438	16,700	8,400
Tungsten	27.5	0.045	0.089	.00075	.00150	14,000	7,000
Zirconium	4.0	0.117	0.234	.00020	.00039	28,600	14,300

(a) The results presented in this table are based on the assumption that the diaphragm is rigidly clamped at its periphery to the diaphragm housing.

Null-Type Diaphragm

In the null-type diaphragm, the magnitude of the diaphragm deflections is not a design consideration and the calibration of the deflections is not necessary. The important considerations are reliability (from the standpoint of failure) and a high natural frequency to avoid resonance. Either a low carbon steel or Type 347 stainless steel would be very desirable because of their high elongation values. Also, the frequency values for both these materials are more than adequate. It is recommended that a 1.0-inch diameter be used for the null-type diaphragm because of the higher frequency of vibration. Actually, any carbon steel or stainless steel with properties at 720 F comparable to those listed in Table 4 could be used for the diaphragm design.

Mechanical-Type Diaphragm

The successful functioning of the mechanical-type diaphragm is partly dependent upon the deflection sensitivity or response of the diaphragm to pressure loading. Also, the deflections should be repeatable at the design temperature. Therefore, a material which creeps at 720 F may not function properly.

The highest deflections are provided by a 2.0-inch-diameter, 6Al-4V titanium or 4340 steel diaphragm. The creep rates for these materials at 720 F are extremely low. However, since the design creep requirements for successful operation of the diaphragm are very stringent, the use of these materials is not recommended.

The temperature below which a material will not creep can be considered a function of the melting point of the material. From Table 4, the high-melting-point materials are molybdenum, tantalum, and tungsten, and considering these metals, the maximum deflection possible is with a 2.0-inch-diameter tungsten diaphragm. This is the recommended design for a mechanical-type diaphragm. The natural frequency of 8400 cycles per second is sufficiently high and the 10 per cent elongation of tungsten at 720 F is adequate. However, it would be desirable to check the elongation of the specific tungsten sheet stock used for the diaphragm.

Choice for Further Analysis

Reviewing the above considerations, it has been decided to limit the development on this program to null-type diaphragms applicable to pneumatic sensing. Thus, the design of the sensor now in study can be portrayed as shown in Figure 2. Thermal expansions must be allowed for in charging the sensor.

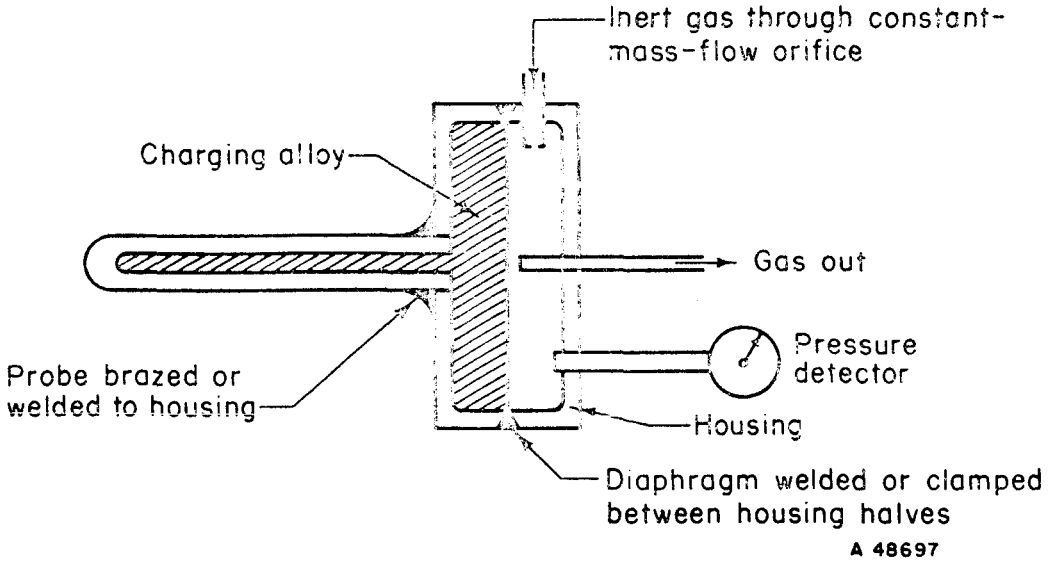

FIGURE 2. PNEUMATIC SENSOR

THERMAL ANALYSIS

Response

To elucidate further the effects of radiative heat loss and internal heat generation on response, the results given in the last quarterly report[1] (obtained from the simplified model, assuming no radial temperature gradients in the probe) have been related to time constant. If we define the time constant as the length of time required for the temperature difference between the gas temperature and the probe temperature to change by a factor of 1/e, it can easily be shown that the time constant for a probe which has only convective interchange with the environment is equal to $\rho C_p L/h$.* If radiative heat loss is introduced, the nonlinearity causes the effective time constant to be a function of temperature and whether or not the probe is heating or cooling. Figure 3 is a plot of the ratio of the effective time constant to $\rho C_p L/h$ versus a normalized probe temperature for heating and cooling with a typical value of the ratio of convective-heat-transfer coefficient to a potential radiation loss parameter, $\sigma\epsilon T_f^{3}$**. The difference between heating and cooling is significant. The effect of radiation is shown in more detail in Figure 4 with heating curves for different values of $h/\sigma\epsilon T_f^{3}$. Cooling curves are not shown, but Figure 3 illustrates that cooling response is more rapid than heating.

Internal generation is introduced in Figure 5. An internal generation parameter, qL/hT_f***, is varied while $h/\sigma\epsilon T_f^{3}$ is held constant at 5. Internal generation aids

(1) Van Orsdel, J. R., et al., "Development of a Vapor-Pressure-Operated High-Temperature Sensor Device", First Quarterly Report, BATT-4673-T2, June 11, 1964.

*ρ-average density of probe materials, C_p = average specific heat of probe materials, L = ratio of volume of probe to surface area, h = convective-heat-transfer coefficient.

**σ = Stefan-Boltzmann constant, ϵ = emissivity of probe surface, T_f = temperature of gas stream (absolute units).

***q = internal heat-generation rate per unit volume.

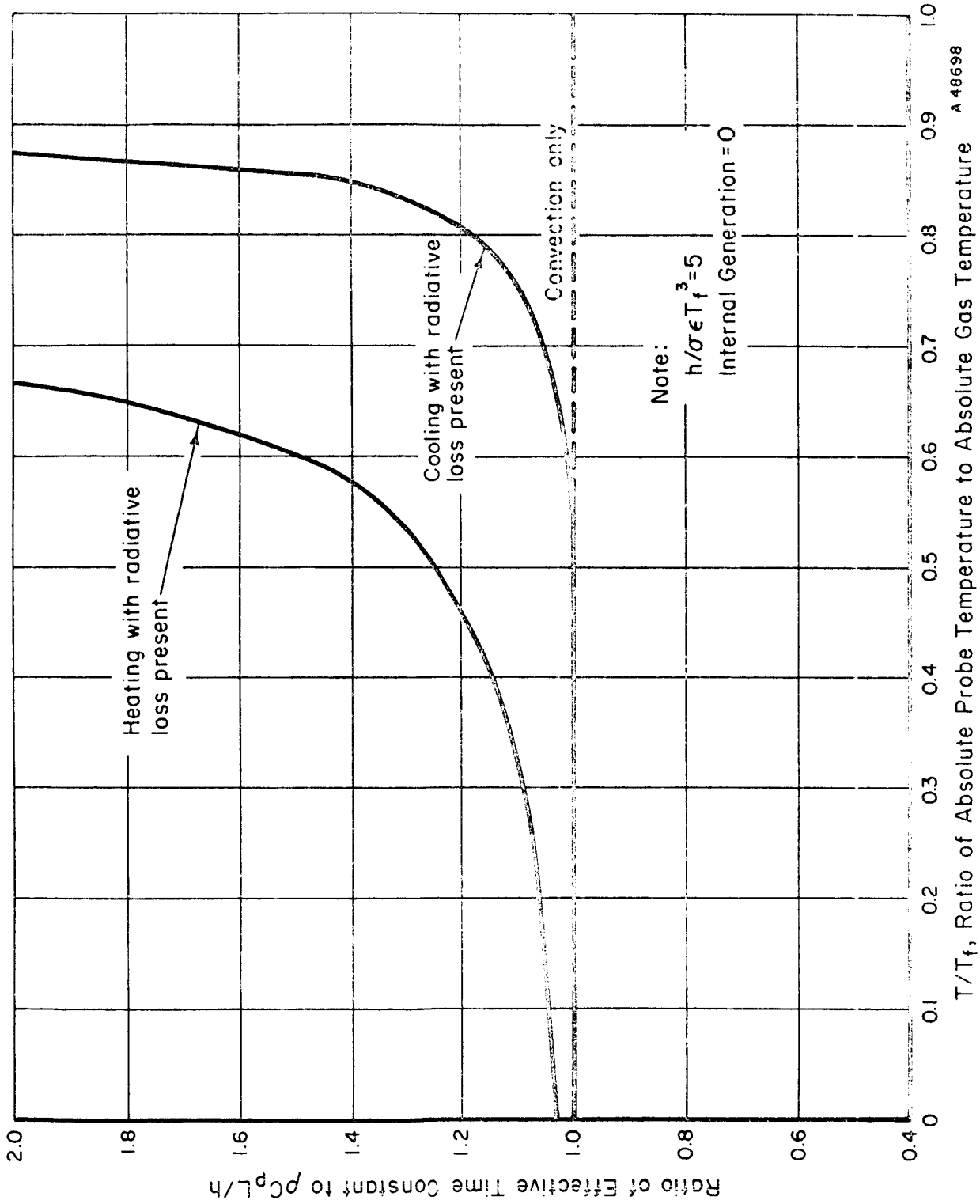

FIGURE 3. ILLUSTRATION OF THE DIFFERENCE IN RESPONSE ON HEATING OR COOLING WHEN RADIATIVE LOSS IS PRESENT

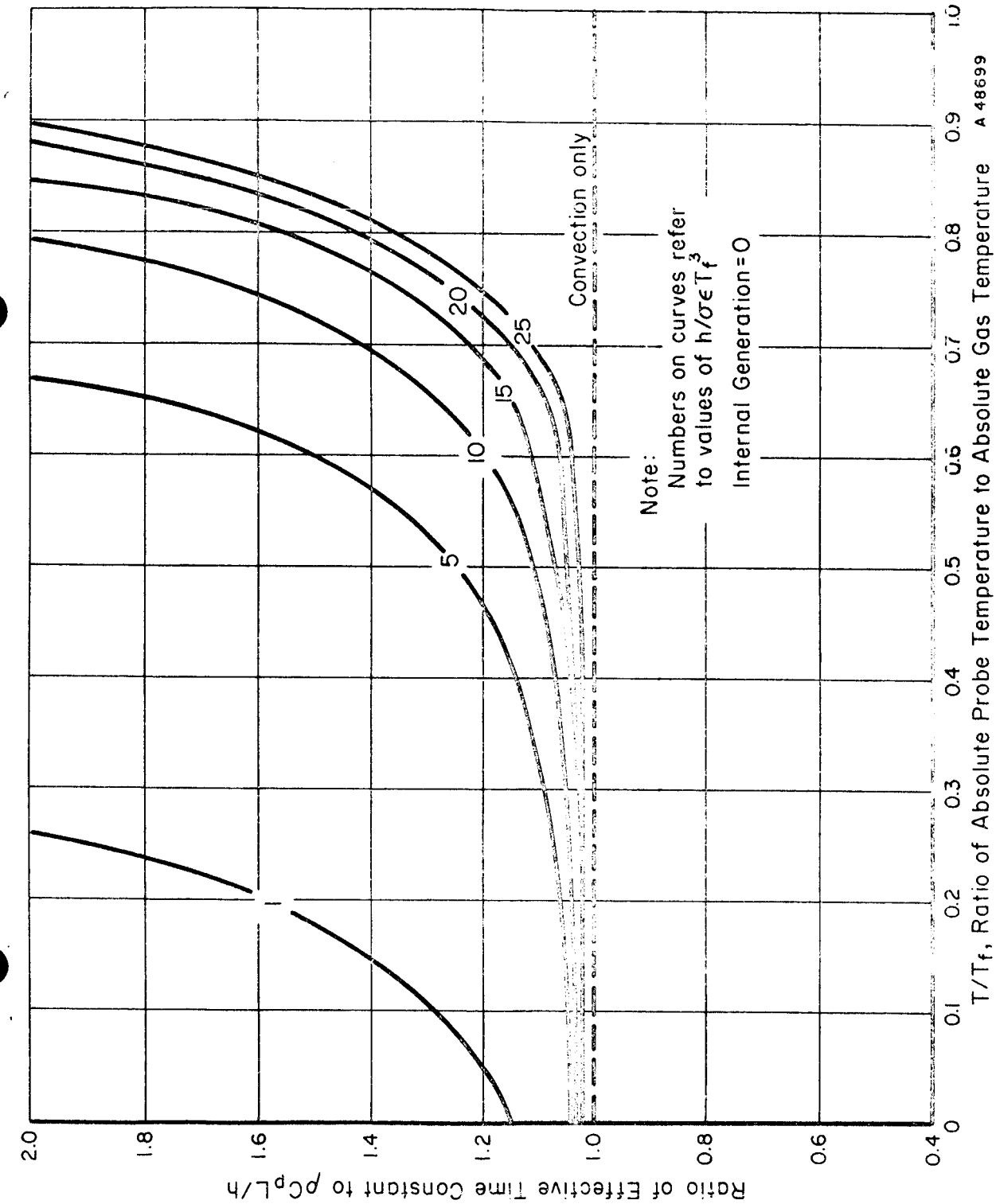

FIGURE 4. THE EFFECT OF RADIATIVE LOSS ON THE EFFECTIVE TIME CONSTANT WHEN HEATING

response on heating, and although cooling curves have not been calculated, it would hinder response on cooling. Values of 0.04 and 5 are considered typical of the internal generation and convection/radiation parameters, respectively, for the planned application. Examination of this typical curve on Figure 5 shows that a probe with a nominal time constant of 1/2 second would respond initially (on heating) with an effective time constant of about 0.48 second. When the temperature is about 0.4 times the gas temperature, i.e., about 2000 R if gas temperature is about 5000 R, the effective time constant is up to 1/2 second. It would gradually increase to about 0.75 second at about 3500 R, and would rise very rapidly above 3500 R because the steady-state temperature for this particular case is less than the gas temperature. This illustrates that the probe would tend to be rather sluggish in following minor changes at high temperatures. However, this response characteristic is not confined to the probe under study but would also be true for a thermocouple of like size and material.

These results from the simplified model of course neglect the effect of the finite thermal conductivities of the probe materials. To consider this effect, a one-dimensional (radial) finite-difference transient-heat-transfer program has been developed. This program accommodates the multiregion, radiative-convective boundary case and will be available for parametric runs in the near future. Discussion of this problem will be postponed until results pertinent to this application are available.

Conduction Losses Along the Length of the Probe

The importance of axial conduction as related to length of the probe has been considered using Battelle's two-dimensional steady-state heat-transfer program which will accept cylindrical geometry. The significant results of this study are shown in Figure 6. Table 6 illustrates the input data for the four cases. For surface temperatures less than the gas temperature, the convective input is greater than the internal heat generation; therefore temperatures decrease from the surface inward. Thus the maximum liquid-metal temperature at a given axial location is usually along the solid-liquid interface. These are the curves shown in Figure 6 for the four cases that were studied. These curves show that the axial heat loss may be neglected if the length of the probe is about four times its diameter. The calculated radial temperature differences (surface temperature minus center-line temperature) at the end cap-liquid metal interface for the four cases are 108, 36, 5, and -4 F for 1:1, 2:1, 3:1, and 4:1 length-to-diameter ratios, respectively; this also indicates the advantage of a long probe.

The computer program does not permit radiative boundaries. Radiative loss was approximately accounted for by applying a convective coefficient on the cylindrical surface equivalent to radiative loss at a surface temperature of 4000 R, in addition to the normal convective heat input from the hot gas. This is obviously in significant error so that the curves of Figure 6 should be used only by comparison of lengths. The probable steady-state error in the temperature should not be obtained from this graph (see last quarterly instead). A hypothetical curve is sketched on Figure 6 illustrating qualitatively the proper effect of radiative loss on the temperature profile.

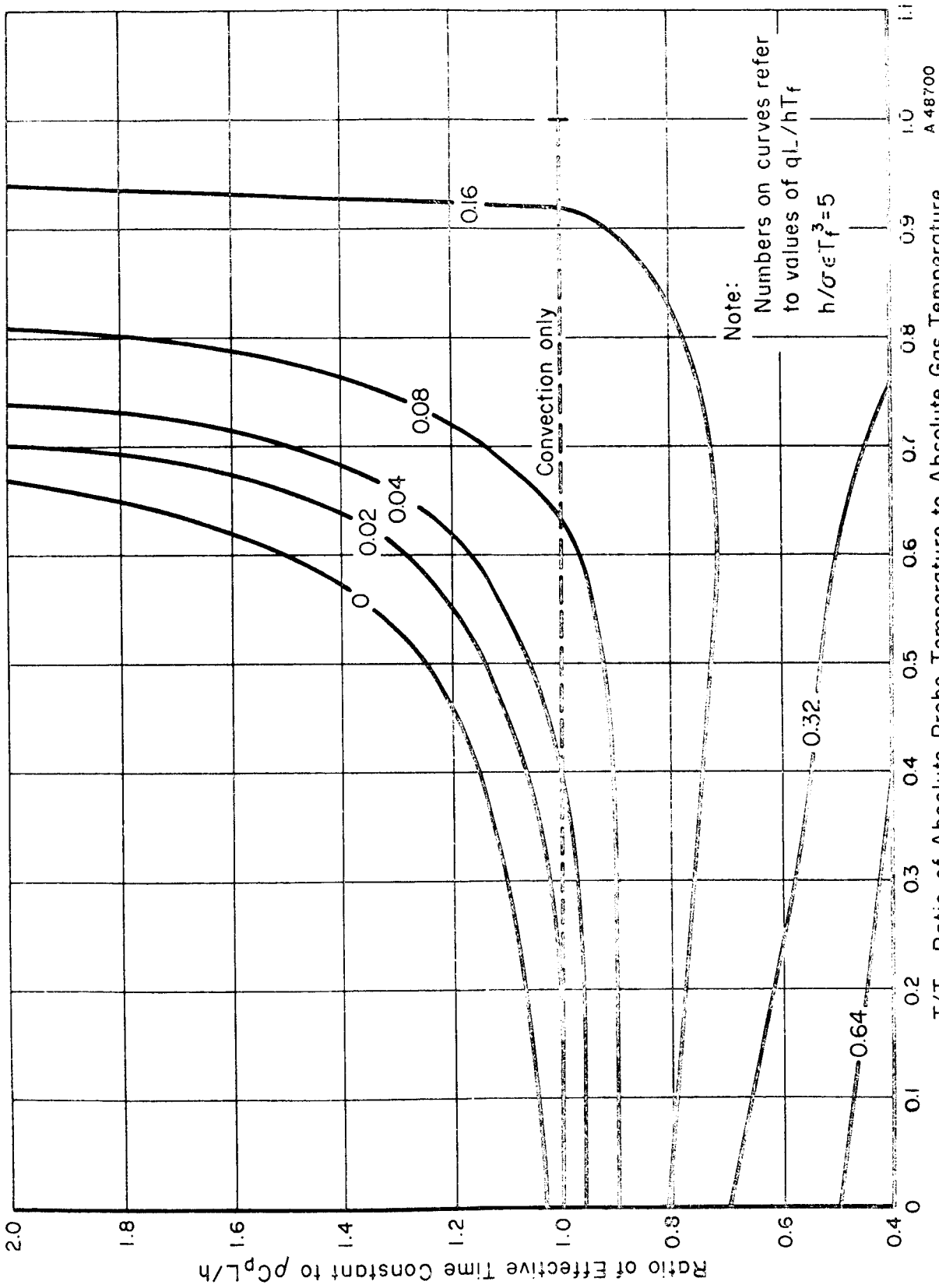

FIGURE 5. THE EFFECT OF INTERNAL HEAT GENERATION ON THE EFFECTIVE TIME CONSTANT WHEN HEATING WITH NOMINAL RADIATIVE LOSS PRESENT

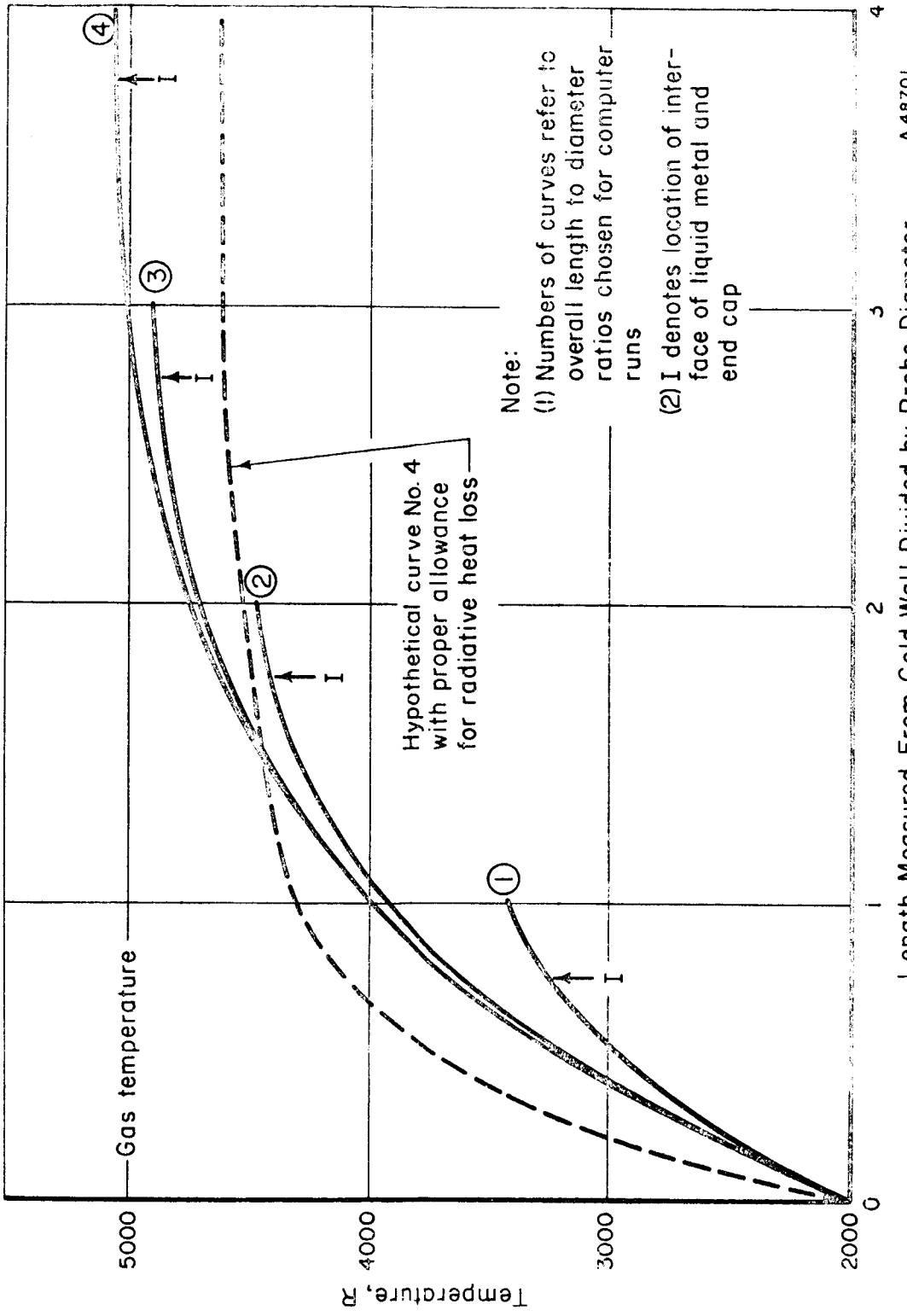

FIGURE 6. EFFECT OF PROBE LENGTH ON STEADY STATE AXIAL TEMPERATURE PROFILE ALONG SOLID METAL WALL

TABLE 6. INPUT PARAMETERS FOR AXIAL-HEAT-LOSS STUDY

Materials	
Container	Tungsten
Liquid Metal	Lead
Outside Diameter	1/4 inch
Wall Thickness	1/16 inch
End-Cap Thickness	1/16 inch
Thermal Conductivities	
Lead	20 Btu/(hr)(ft)(F)
Tungsten	48 Btu/(hr)(ft)(F)
Gamma-Heat-Generation Rates	
Lead	10 watts/g $\begin{cases} 1.0 \times 10^7 \text{ Btu/(hr)(ft}^3\text{)} \\ 1.7 \times 10^7 \text{ Btu/(hr)(ft}^3\text{)} \end{cases}$
Tungsten	
Cold-End Temperature	2000 R
Gas Temperature	5000 R
Emissivity of Tungsten	0.3
Convective Coefficient	1000 Btu/(hr)(ft^2)(F)

During this study it was also shown that the axial-loss behavior of the probe is not greatly dependent on the wall thickness for a tungsten-lead combination. If one considers the steady-heat-conduction equation:

$$k_i\left(\frac{\partial^2 T_i}{\partial r^2} + \frac{1}{r}\frac{\partial T_i}{\partial r} + \frac{\partial^2 T_i}{\partial z^2}\right) = q_i \text{ *}.$$

The subscript, i, is either 1 or 2 referring to tungsten or lead. If the above equation is divided through by k_i, it is apparent that the system can be considered as one physical region with a "pseudo" thermal conductivity of 1, and a "pseudo" heat generation rate of q_i/k_i. Inspection of Table 6 reveals that the ratio q_i/k_i is crudely the same for either material. This conclusion may also be drawn concerning a tungsten-bismuth system, since the equality of q_i/k_i ratios is more closely approximated.

Further studies of axial heat loss are not planned.

FUTURE WORK

Probe testing will be continued at high temperature with the use of hydrogen under pressure around the exterior of the probe. A test will then be made to determine whether hydrogen diffused into the probe in significant quantities.

Extended time tests with temperature cycling will be conducted for further proof tests of probe life.

A simple laboratory test of a pneumatic sensing element will be conducted to evaluate the suitability and time response associated with such a diaphragm device. A 2-inch diaphragm will be assembled, with provisions for restricting the active diameter to 1 inch, such that both diameters can be evaluated in the same housing.

Future thermal analyses will consider the effect of the finite thermal conductivities of probe materials on thermal response utilizing the transient program developed this quarter.

JRV/GER/JMA:so

*k = thermal conductivity, T = temperature, r = radial direction, z = axial direction.

APPENDIX A

METALLOGRAPHY

APPENDIX A

METALLOGRAPHY

Photomicrographs showing the effects of high temperature on the compatibility of container materials and charging metals are presented in this appendix.

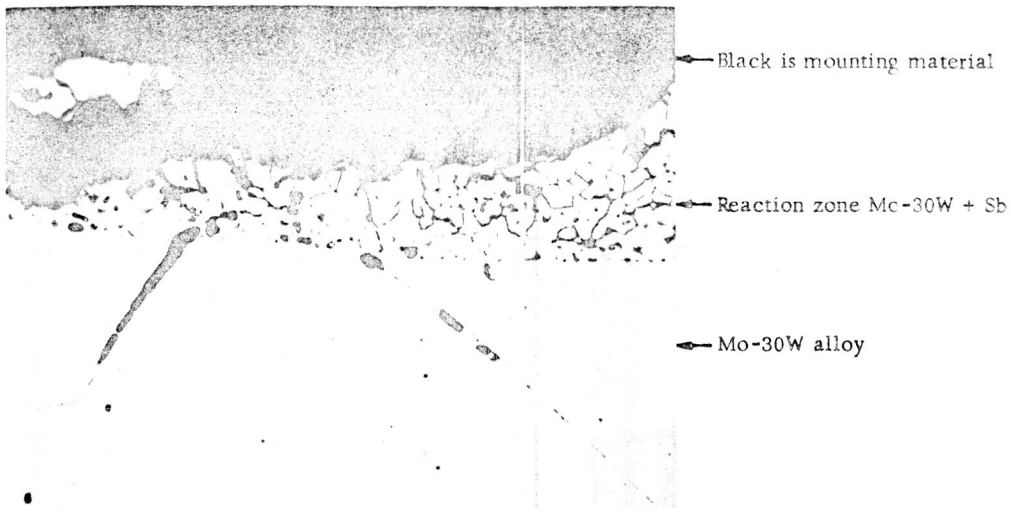

250X Light Murakami's Etch 14480

FIGURE A-1. COMPATIBILITY OF Mo-30W AND ANTIMONY AT 4500 R FOR 5 MINUTES

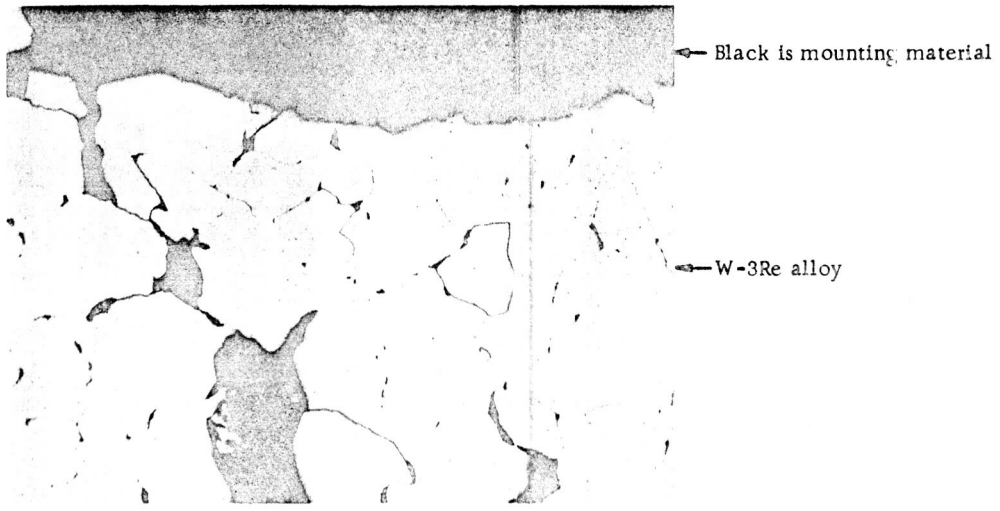

100X Light Murakami's Etch 14481

FIGURE A-2. COMPATIBILITY OF W-3Re ALLOY AND BISMUTH AT 4500 R FOR 3 MINUTES, SHOWING SEVERE GRAIN-BOUNDARY ATTACK BY BISMUTH, RESULTING IN RUPTURE OF SPECIMEN

Bismuth vaporized and is not present in failure.

FIGURE A-3. COMPATIBILITY OF W-3Re ALLOY AND ANTIMONY AT 4500 R FOR 1 HOUR

Though no rupture occurred, grain-boundary penetration was severe and rupture was imminent.

FIGURE A-4. COMPATIBILITY OF W-3Re ALLOY AND ANTIMONY AT 5000 R

Specimen ruptured in about 5 minutes.

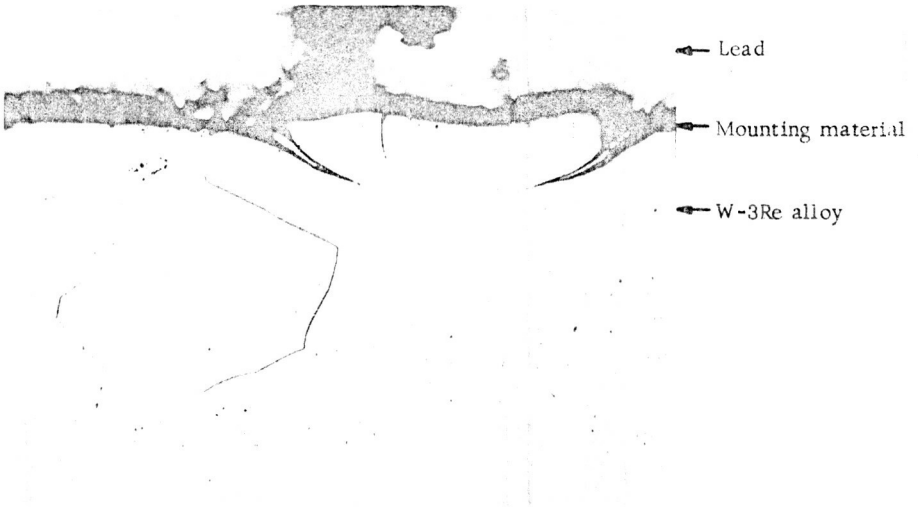

250X Light Murakami's Etch 14485

FIGURE A-5. COMPATIBILITY OF W-3Re ALLOY AND LEAD AT 4500 R FOR 1 HOUR

Attack is slight. Depth of lead penetration about 0.002 inch.

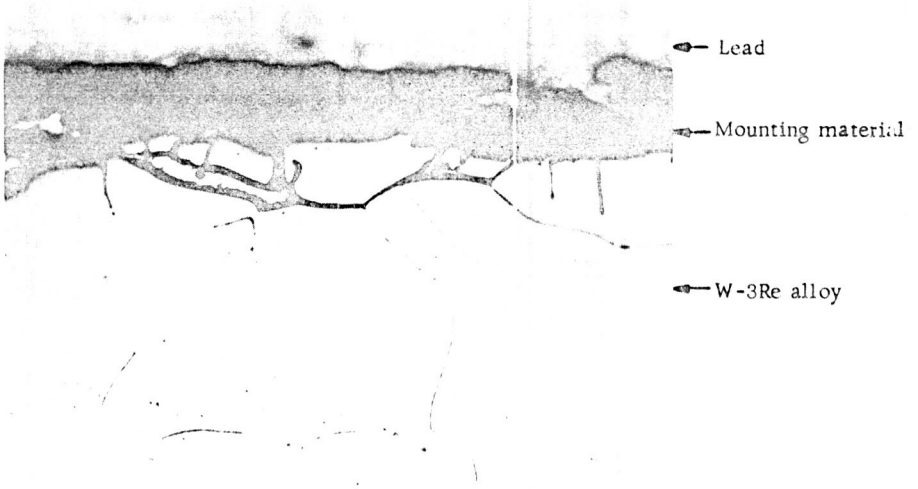

250X Light Murakami's Etch 14486

FIGURE A-6. COMPATIBILITY OF W-3Re ALLOY AND LEAD AT 5000 R FOR 1 HOUR

Grain-boundary attack stronger than at 4500 R, but maximum penetration only about 0.0025 inch.

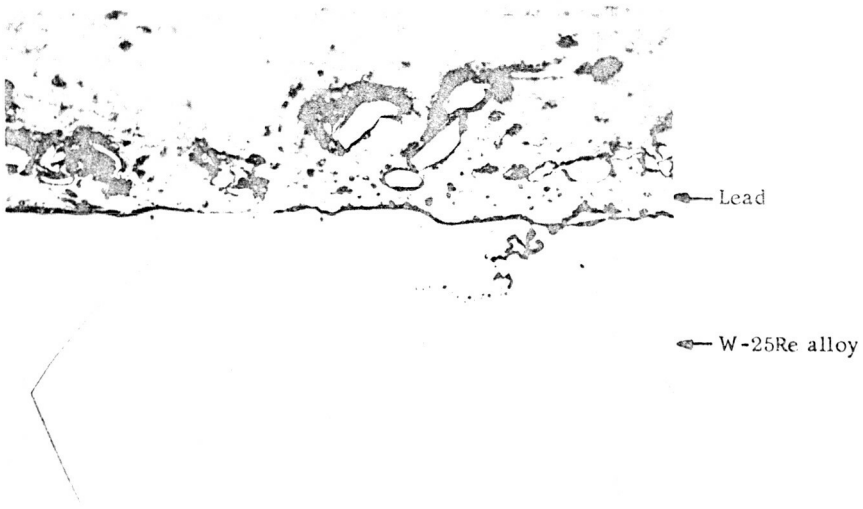

250X Murakami's Etch 15085

FIGURE A-7. COMPATIBILITY OF W-25Re ALLOY AND LEAD AT 4500 R FOR 1 HOUR

Attack is considered minor. Angular particles are believed to be remnants from the rough base.

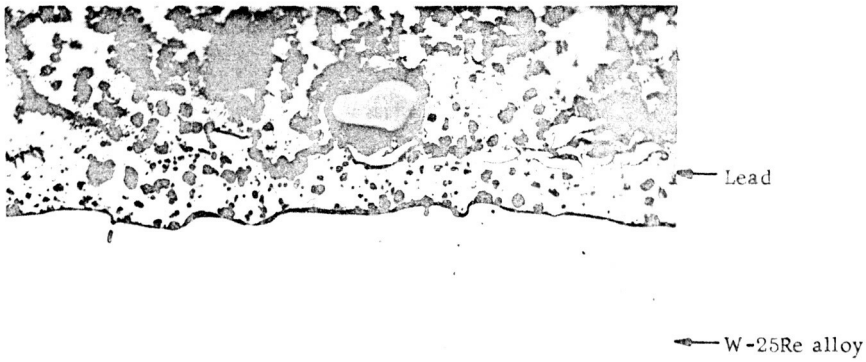

250X Murakami's Etch 15086

FIGURE A-8. COMPATIBILITY OF W-25Re ALLOY AND LEAD AT 5000 R FOR 1 HOUR

Lead shows porosity in this area and a few fragments of W-Re alloy.

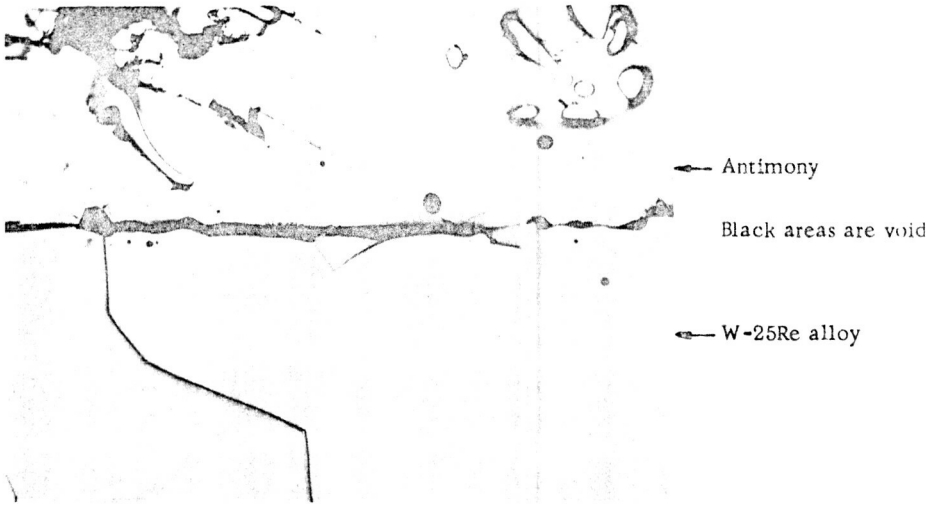

250X Murakami's Etch 15087

FIGURE A-9. COMPATIBILITY OF W-25Re ALLOY AND ANTIMONY AT 4500 R FOR 1 HOUR

Attack by antimony appears minor.

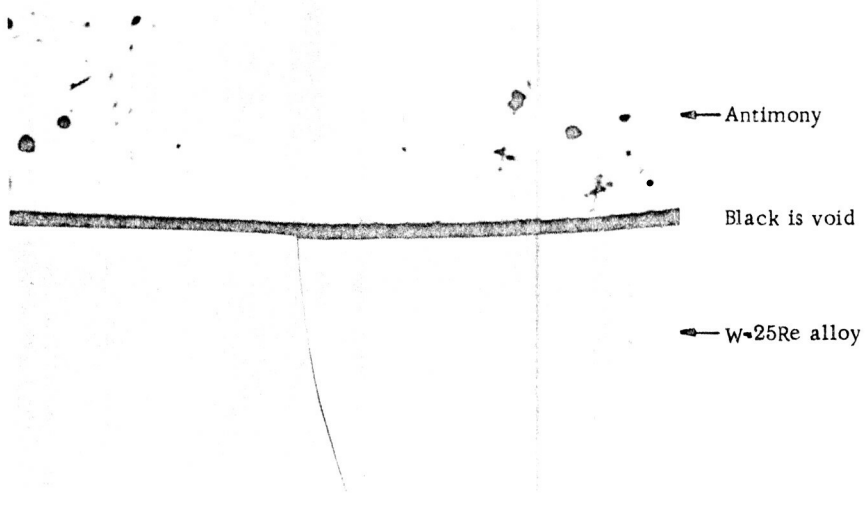

250X Murakami's Etch 15088

FIGURE A-10. COMPATIBILITY OF W-25Re ALLOY AND ANTIMONY AT 5000 R FOR 1 HOUR

Reaction between the two metals appears absent. However, the sample expanded about 2.4 per cent in diameter owing to creep.

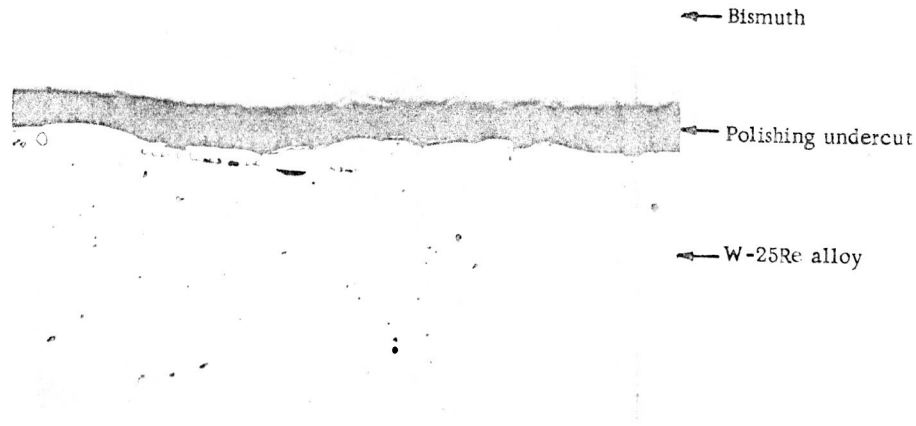

250X Murakami's Etch 15089

FIGURE A-11. COMPATIBILITY OF W-25Re ALLOY AND BISMUTH AT 4500 R FOR 1 HOUR

Shows only very slight attack.

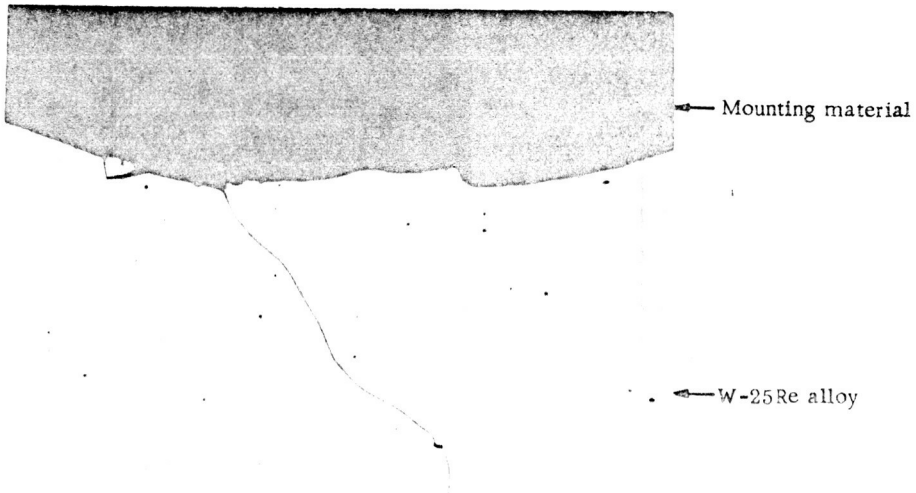

250X Murakami's Etch 15090

FIGURE A-12. COMPATIBILITY OF W-25Re ALLOY AND BISMUTH AT 5000 R FOR 50 MINUTES

Sample burst in creep and bismuth was vaporized. Bismuth is not believed to have attacked the W-25 Re alloy.

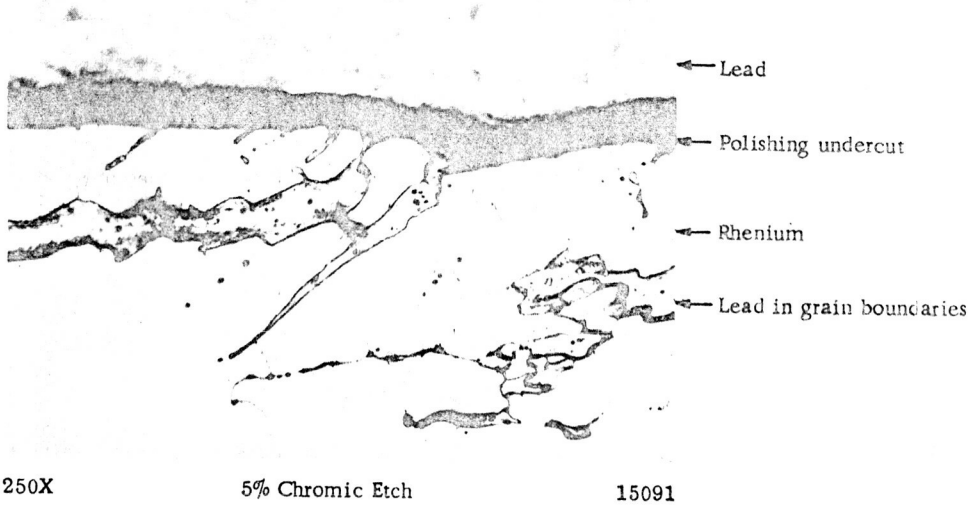

250X 5% Chromic Etch 15091

FIGURE A-13. COMPATIBILITY OF RHENIUM AND LEAD AT 5000 R FOR 1 HOUR

Penetration of grain boundaries by lead is evident though sample did not fail.

250X 5% Chromic Etch 15092

FIGURE A-14. COMPATIBILITY OF RHENIUM AND BISMUTH AT 5000 R FOR 1 HOUR

Grain-boundary attack is severe but failure did not occur.